Article

Cell Reports

Decrease of a Current Mediated by $K_v1.3$ Channels Causes Striatal Cholinergic Interneuron Hyperexcitability in Experimental Parkinsonism

Graphical Abstract

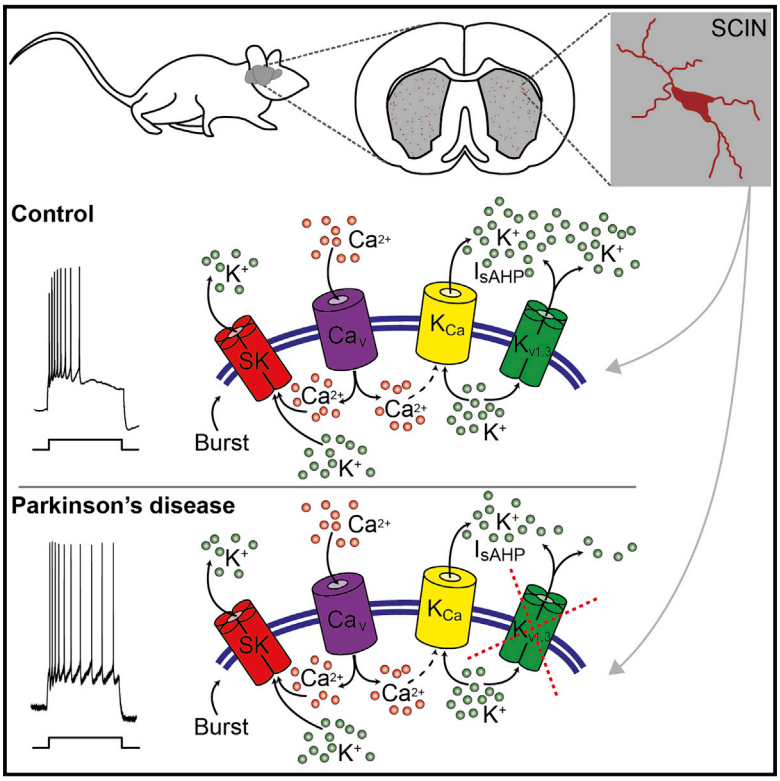

Authors

Cecilia Tubert, Irene R.E. Taravini, Eden Flores-Barrera, ..., Kuei Y. Tseng, Lorena Rela, Mario Gustavo Murer

Correspondence

cecitubert@gmail.com

In Brief

The mechanisms underlying the hypercholinergic state of Parkinson's disease remain uncertain. Tubert et al. show that $K_v1.3$-containing channels limit firing and contribute to I_{sAHP} in striatal cholinergic interneurons. The $K_v1.3$ current decreases in a mouse model of Parkinson's disease, spotting $K_v1.3$-containing channels as potential targets for Parkinson's disease therapy.

Highlights

- $K_v1.3$ channels control SCIN excitability and synaptic integration
- $K_v1.3$ current is a non-canonical component of the orphan current I_{sAHP} in SCINs
- SCINs become hyperexcitable in a mouse Parkinson's disease model
- SCIN $K_v1.3$ current is markedly reduced in the parkinsonian state

Tubert et al., 2016, Cell Reports *16*, 2749–2762
September 6, 2016
http://dx.doi.org/10.1016/j.celrep.2016.08.016

Cell Reports
Article

Decrease of a Current Mediated by $K_v1.3$ Channels Causes Striatal Cholinergic Interneuron Hyperexcitability in Experimental Parkinsonism

Cecilia Tubert,[1,6,*] Irene R.E. Taravini,[2] Eden Flores-Barrera,[3] Gonzalo M. Sánchez,[1,5] María Alejandra Prost,[1] María Elena Avale,[4] Kuei Y. Tseng,[3] Lorena Rela,[1] and Mario Gustavo Murer[1]
[1]IFIBIO Bernardo Houssay, Grupo de Neurociencia de Sistemas, Facultad de Medicina, Universidad de Buenos Aires - CONICET, 2155 Paraguay Street, Buenos Aires 1121, Argentina
[2]Neurobiología Experimental, Universidad de Entre Ríos, Gualeguaychú, Entre Ríos E2822EXB, Argentina
[3]Department of Cellular and Molecular Pharmacology, The Chicago Medical School at Rosalind Franklin University, Chicago, IL 60064, USA
[4]Instituto de Investigaciones en Ingeniería Genética y Biología Molecular (INGEBI), CONICET, Buenos Aires 1428, Argentina
[5]Present address: Division of Cell Biology, Department of Clinical and Experimental Medicine (IKE), Linköping University (CELLB), Linköping 581-83, Sweden
[6]Lead Contact
*Correspondence: cecitubert@gmail.com
http://dx.doi.org/10.1016/j.celrep.2016.08.016

SUMMARY

The mechanism underlying a hypercholinergic state in Parkinson's disease (PD) remains uncertain. Here, we show that disruption of the K_v1 channel-mediated function causes hyperexcitability of striatal cholinergic interneurons in a mouse model of PD. Specifically, our data reveal that K_v1 channels containing $K_v1.3$ subunits contribute significantly to the orphan potassium current known as I_{sAHP} in striatal cholinergic interneurons. Typically, this K_v1 current provides negative feedback to depolarization that limits burst firing and slows the tonic activity of cholinergic interneurons. However, such inhibitory control of cholinergic interneuron excitability by $K_v1.3$-mediated current is markedly diminished in the parkinsonian striatum, suggesting that targeting $K_v1.3$ subunits and their regulatory pathways may have therapeutic potential in PD therapy. These studies reveal unexpected roles of $K_v1.3$ subunit-containing channels in the regulation of firing patterns of striatal cholinergic interneurons, which were thought to be largely dependent on K_{Ca} channels.

INTRODUCTION

Parkinson's disease (PD) is caused by the degeneration of dopamine-producing neurons that preferentially project to the striatum. Its management is mostly based on the symptomatic effect of drugs that increase the stimulation of dopamine receptors in the striatum and other structures (Kalia and Lang, 2015). Motor function depends on a balance between dopamine and acetylcholine, another important modulator of striatal function (Barbeau, 1962; Cragg, 2006; Pisani et al., 2007). According to a classical view, the loss of dopamine inhibitory actions on acetylcholine release leads to a hypercholinergic state in PD (Barbeau, 1962). It is now accepted that interactions between striatal dopamine and acetylcholine are far more complex than previously thought (Wang et al., 2006; Threlfell et al., 2012; Nelson et al., 2014). However, anticholinergics were the drugs of choice for PD management before the discovery of the symptomatic effect of L-DOPA (Barbeau, 1962), and they are still considered efficacious for its treatment (Kalia and Lang, 2015). Recent studies further support that striatal acetylcholine plays a significant role in PD pathophysiology (Ding et al., 2006, 2011; Sanchez et al., 2011; Maurice et al., 2015). Thus, preventing changes of striatal acetylcholine may have therapeutic potential in PD (Deffains and Bergman, 2015).

The main source of striatal acetylcholine is a small population of striatal cholinergic interneurons (SCINs) with tonic activity. Nevertheless, the striatum has very high levels of acetylcholine, choline acetyltransferase (ChAT), acetylcholinesterase, and cholinergic receptors (Cragg, 2006; Pisani et al., 2007). The tonic activity of SCINs is intrinsically generated (Bennett and Wilson, 1999). During an action potential, Ca^{2+} entry through voltage-dependent Ca^{2+} channels (Ca_v) activates large-conductance (BK) and small-conductance (SK) Ca^{2+}-dependent K^+ channels (K_{Ca}). The resulting medium duration after-hyperpolarization (mAHP) activates the depolarizing current I_h, which impels the cell to threshold again (Goldberg and Wilson, 2005; Deng et al., 2007). Bursts of action potentials recruit additional K^+ currents, resulting in a slow AHP (sAHP) and a long pause that interrupts tonic firing (Wilson and Goldberg, 2006). Previous work has identified a deficient inhibitory control of SCIN tonic activity by M4 acetylcholine autoreceptors (Ding et al., 2006) and D_2 dopamine receptors (DeBoer et al., 1996; Maurice et al., 2004) as putative mechanisms underlying a rise in acetylcholine release in PD. Moreover, we have reported that a component of the current underlying sAHP (I_{sAHP}) is diminished in the rat 6-hydroxydopamine (6-OHDA) lesion model of PD, resulting in a dramatic increase of membrane excitability (Sanchez et al., 2011). The

molecular entity underlying I_{sAHP} has remained unknown for decades (Andrade et al., 2012), precluding the identification of the K^+ channels involved in SCIN hyperexcitability.

Although it often has been assumed that I_{sAHP} is mediated by a specific K_{Ca} channel, recent studies suggest that different ion channels could be involved in different neuron types (Andrade et al., 2012; King et al., 2015). In SCINs, the I_{sAHP} is described as a K_{Ca} current linked to Ca^{2+} entry through dihydropyridine (DHP)-sensitive Ca_v channels (Goldberg and Wilson, 2005). Here, we report that a decrease of a delayed rectifier type K_v current that prominently regulates SCIN excitability causes the hyperexcitability observed after a chronic nigrostriatal lesion. Furthermore, we demonstrate that these K_v channels contribute to the current evoked by protocols used to assess I_{sAHP}, supporting that K_v and K_{Ca} channels mediate I_{sAHP} in SCINs.

RESULTS

To facilitate the localization of SCINs in brain slices, we used transgenic mice in which the expression of the fluorescent protein tdTomato is under the control of *Chat* regulatory sequences (ChAT-Cre;tdT) (Figure S1). The tdTomato-positive striatal neurons of these animals (Figure 1A) exhibit the following electrophysiological signatures of SCINs (Table S1): (1) spontaneous firing activity (Figure 1B); (2) a sag in response to hyperpolarizing current injection (Figure 1C); (3) a slowing of discharge rate (spike frequency adaptation) commonly followed by a complete stop of firing (accommodation) in response to depolarizing current injection (Figures 1C and 1D); (4) a rebound depolarization after a hyperpolarizing current step (Figure 1C); and (5) an sAHP following a depolarizing current step (Figure 1C) (Sanchez et al., 2011; Bennett and Wilson, 1999; Jiang and North, 1991; Maurice et al., 2004).

Accommodation is observed in most, but not all SCINs. To characterize the different phenotypes of SCIN excitability, firing patterns in response to 1-s duration current steps were recorded from SCINs of juvenile (14- to 45-day-old) and adult (60- to 180-day-old) mice. Regardless of age, most SCINs showed either accommodation or sustained firing (Figure 1E) across the range of depolarizing currents tested. Mixed patterns, accommodation at high, but not low, current intensities or vice versa, were infrequent (Figure 1F). Moreover, non-accommodating SCINs did not stop firing, and accommodating SCINs did not restart firing, when current injection was sustained for 2 s (Figure 1E). Finally, accommodation was not due to depolarization block since current oversteps induce firing at times when step-induced firing already has accommodated (Figure 1C).

To unbiasedly distinguish accommodating from non-accommodating SCINs, last spike time and the number of spikes fired during the 1-s pulse were taken as indexes of the presence and strength of accommodation. Unsupervised multivariate clustering distinguished SCINs with short last spike times and low excitability from a cluster of highly excitable SCINs with long last spike times (Figures 1G and S2). Within this cluster the proportion of non-accommodating SCINs differed between the age groups (Figures 1H and S2); 43 of 175 juvenile SCINs were classified as non-accommodating compared with five of 56 in the adult mice ($p = 0.03$, Fisher's exact test). On average, in juvenile mice, non-accommodating SCINs fired 10.4 ± 0.7 spikes in 831 ± 16 ms and accommodating SCINs fired 5.1 ± 0.2 spikes in 367 ± 12 ms (Figure 1G), whereas in adult mice, non-accommodating and accommodating SCINs fired 9.6 ± 2.2 spikes during 810 ± 55 ms and 4.4 ± 0.3 spikes during 340 ± 20 ms, respectively. Importantly, accommodating and non-accommodating SCINs showed similar resting membrane potential, action potential threshold, amplitude and duration, sag and sAHP amplitudes, and input resistance (Table S2), but they differed in that the rheobase current was smaller in non-accommodating (28 ± 4 pA) than in accommodating SCINs (54 ± 7 pA; $p = 0.002$, t test).

In summary, SCINs can be classified into two types based on their firing pattern in response to a current step, and maturation into adulthood is characterized by an increase in the proportion of accommodating SCINs.

$K_v1.3$ Subunit-Containing Channels Mediate Accommodation in SCINs

To identify the current that was mediating accommodation, we tested the effect of drugs and toxins that block candidate K_{Ca} and K_v currents on SCIN excitability. The K_{Ca} SK and sAHP currents have a prominent role in sculpting SCIN firing patterns (Goldberg and Wilson, 2005). Moreover, K_{Ca} channels mediate accommodation in several neuron types (Sah and Faber, 2002). Previously we have found that accommodation persists in the presence of apamin, a selective SK channel blocker (Sanchez et al., 2011). Moreover, accommodation is insensitive to blockers of the Ca_v channels that trigger the sAHP current in SCINs (Goldberg and Wilson, 2005; Sanchez et al., 2011). Recent studies suggest that $K_{Ca}3.1$ channels mediate the I_{sAHP} in hippocampal neurons (King et al., 2015). However, SCINs do not express the $K_{Ca}3.1$ mRNA and do not appreciably show $K_{Ca}3.1$ immunoreactivity (Figure S3). SCINs also express K_v7 channels (Cooper et al., 2001), similar to those that mediate I_M-like and I_{sAHP}-like currents (Tzingounis and Nicoll, 2008), and they induce accommodation (Peters et al., 2005; Yue and Yaari, 2004) in other neurons. However, XE-991 (10 μM), a widely accepted K_v7 blocker, had no effect on accommodation in SCINs (Figure S3; Sanchez et al., 2011).

The K_v1 family has been related to accommodation in neurons of the amygdala and other structures (Sciamanna and Wilson, 2011; Dodson et al., 2002; Faber and Sah, 2004), and SCINs express K_v1 channels and currents (Song et al., 1998; Deng et al., 2005) whose physiological roles have received little attention. Toxins isolated from scorpion and snake venoms bind to K_v1 subunits with variable selectivity. Margatoxin (MgTx, 30 nM), which preferentially blocks channels containing $K_v1.3$ subunits (Garcia-Calvo et al., 1993), markedly attenuated accommodation in SCINs (Figure 2A), as shown by an increase in the number of spikes fired and a lengthening of last spike time in response to depolarizing current steps (Figures 2A–2D). α-dendrotoxin (α-DTX, 100 nM), which has some selectivity for $K_v1.1$, $K_v1.2$, and $K_v1.6$ subunits, also reduced accommodation to an extent similar to MgTx, but Tityustoxin, which shows selectivity for the $K_v1.2$ subunit, had no effect (Hopkins, 1998) (Figures 2D and S3). The effects of MgTx and α-DTX on accommodation were

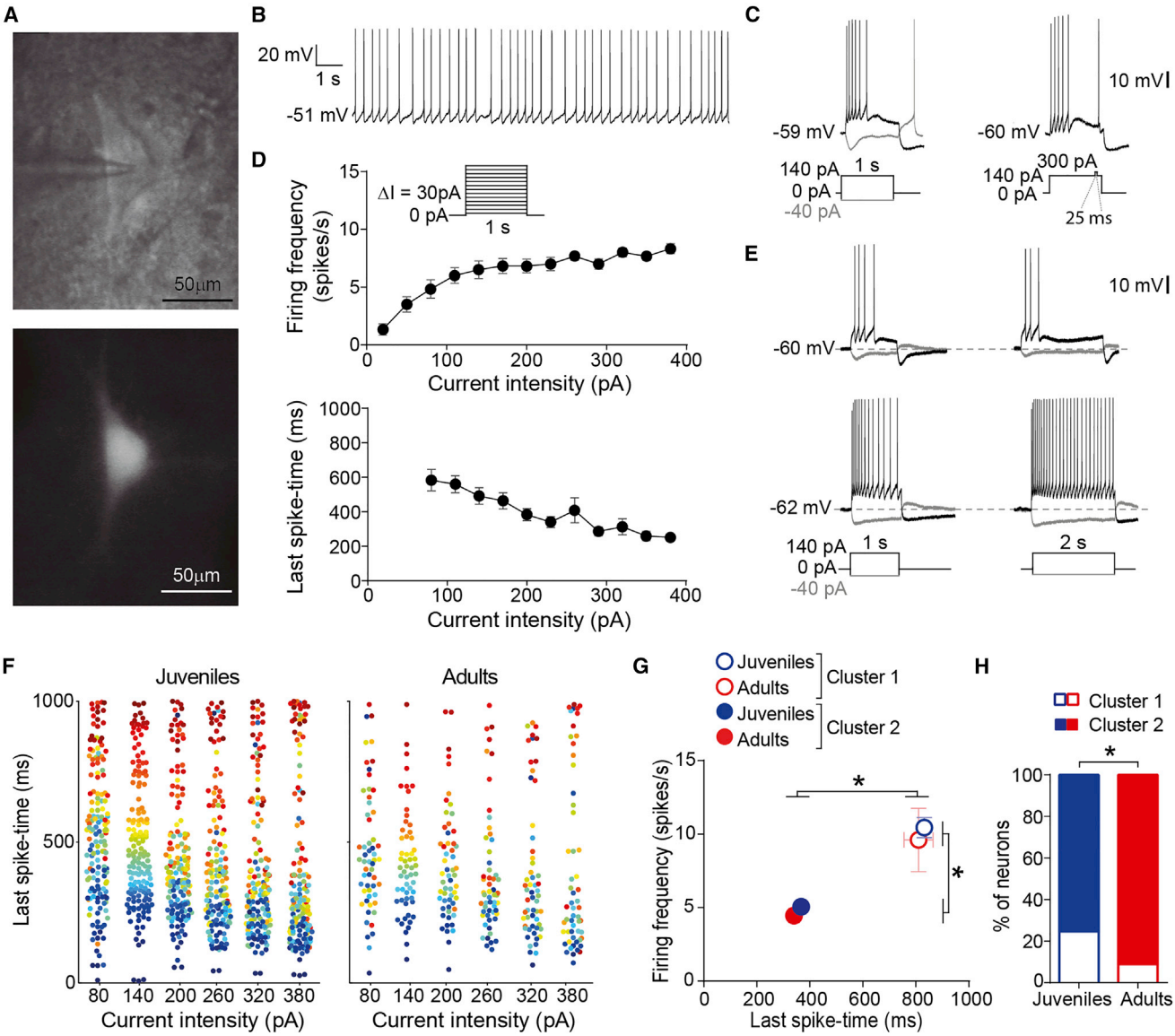

Figure 1. SCIN Excitability Shows Different Phenotypes and Decreases with Age

(A) SCIN from a ChAT-Cre;tdT mouse under differential interference contrast (DIC) (top) and epifluorescent (bottom) illumination is shown.

(B and C) Representative recordings show SCIN spontaneous activity (B) and responses to 1-s current steps (C) with (right) or without (left) overstep at 900 ms.

(D) Firing frequency (top) and last spike time (bottom) versus current intensity during 1-s depolarization (inset). (n = 9 SCINs from six juvenile mice). See Table S1. Data are mean ± SEM.

(E) Responses of accommodating (top) and non-accommodating (bottom) SCINs to 1-s (left) and 2-s (right) current pulses are shown.

(F) Last spike times of SCINs from juvenile (left) and adult (right) mice during 1-s depolarization, color coded from short to long values with the 140-pA pulse, are shown.

(G) Firing frequency versus last spike time (140-pA step) of non-accommodating (cluster 1) and accommodating (cluster 2) SCINs from juvenile and adult mice, as classified by multivariate cluster analysis (*$p < 0.0001$, two-way ANOVA). Data are mean ± SEM.

(H) Percentage of non-accommodating and accommodating SCINs in juvenile and adult mice ($p = 0.03$, Fisher's exact test).

See Figures S1 and S2 and Tables S1 and S2.

highly selective, as they did not modify other physiological properties of SCINs (Tables S3 and S4; Figure S4). Moreover, MgTx had no effect on the excitability of non-accommodating SCINs (Figures 2E and S4). Thus, the data show that K_v1 channels are selectively involved and necessary for accommodation in SCINs.

The contribution of the $K_v1.3$ subunit to accommodation was further investigated with the selective $K_v1.3$ blockers ADWX-1 (autoimmune drug from Wen-Xin group number 1) and agitoxin-2 (Figures 2D and S4), by including an antibody directed against the intracellular domain of $K_v1.3$ in the recording pipette

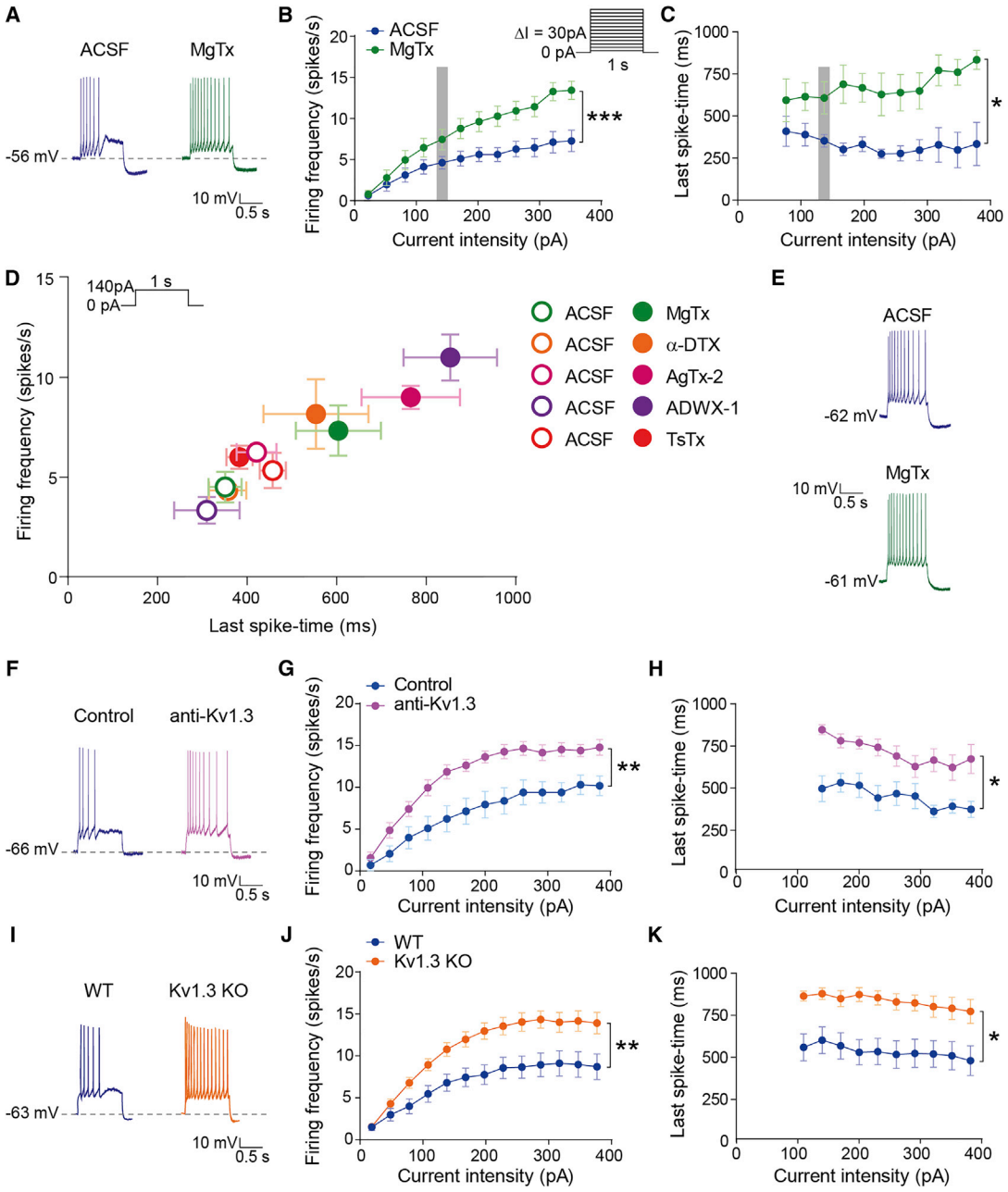

Figure 2. K_v1.3 Channels Control SCIN Excitability

(A) Recording of an accommodating SCIN before and after bath application of 30 nM MgTx is shown.

(B and C) Firing frequency (B) and last spike time (C) versus current intensity before and after adding MgTx are shown (two-way repeated measures [RM] ANOVA interaction, ***$p < 0.0001$ and *$p = 0.049$; n = 6 cells from four juvenile mice).

(D) Firing frequency versus last spike time before and after adding MgTx (30 nM, green), α-DTX (100 nM, orange), AgTx-2 (30 nM, pink), ADWX-1 (10 nM, purple), and TsTx (100 nM, red), is shown.

(E) Response of a non-accommodating SCIN to a 140-pA pulse before and after adding MgTx is shown.

(F–H) Representative SCIN recordings (F) and plots of firing frequency (G) and last spike time (H) versus current intensity, obtained with an anti-K_v1.3 antibody (right; 10 μg/ml, Alomone) or a control antibody (left; 10 μg/ml, biotinylated goat anti-guinea pig, Vector) in the recording pipette, are shown (two-way RM ANOVA interaction, **$p = 0.0002$, anti-Kv1.3 effect: *$p = 0.025$, and current intensity effect: $p = 0.0013$; n = 8–9 cells from two juvenile mice).

(I) Representative recordings show SCINs from wild-type (WT) and K_v1.3 KO mice.

(J and K) Firing frequency (J) and last spike time (K) in SCINs from WT and K_v1.3 KO mice are shown (two-way RM ANOVA interaction, **$p < 0.0001$, genotype effect: *$p = 0.013$ and current intensity effect: $p = 0.0055$; n = 22–24 cells from six mice per group).

Data are mean ± SEM. See Figures S3 and S4 and Tables S3–S5.

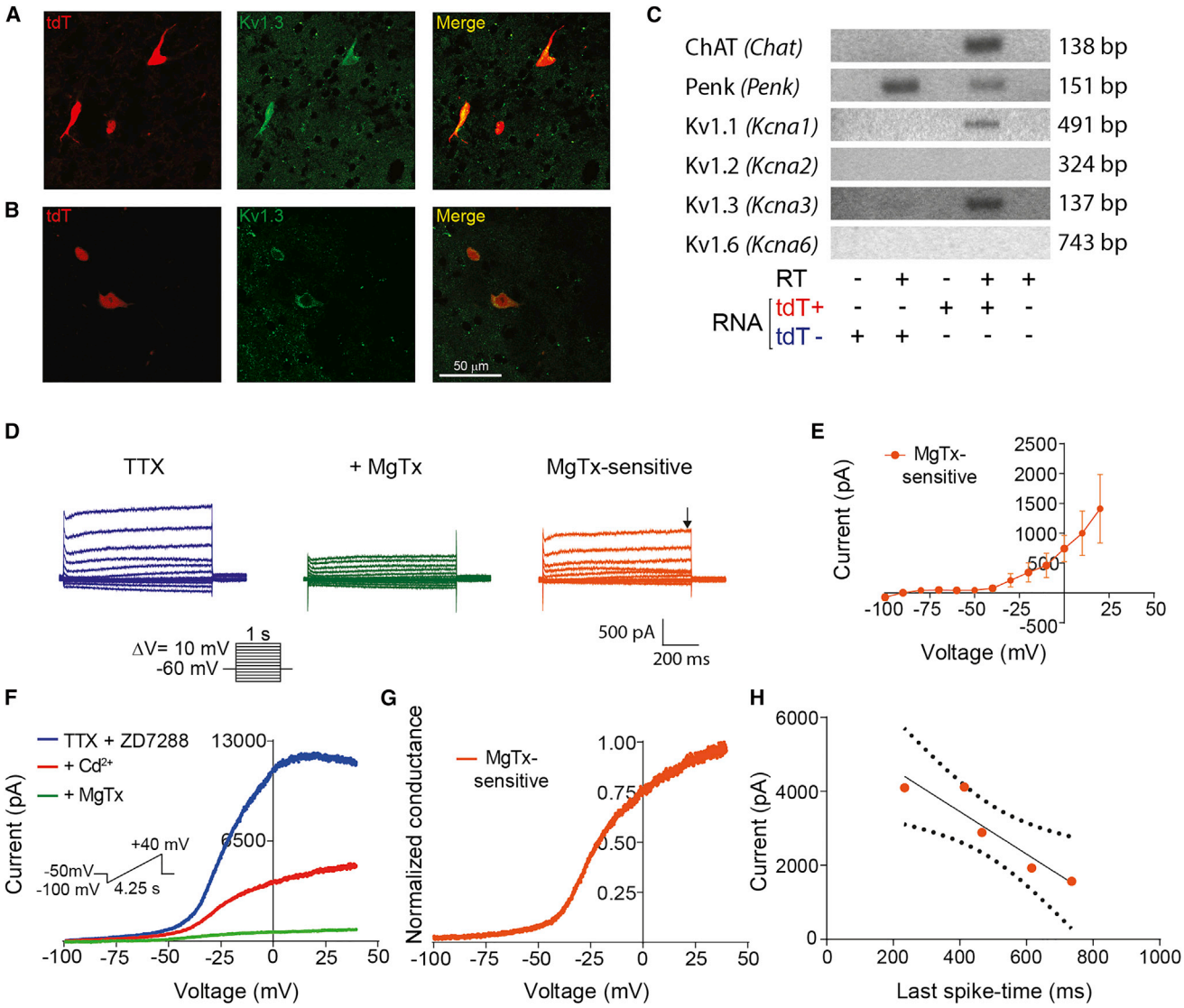

Figure 3. SCINs Express the K_v1.3 Subunit and a MgTx-Sensitive Current

(A and B) Dorsolateral striatal region shows colocalization of tdTomato with K_v1.3 intracellular (A) or extracellular (B) domain immunoreactivity.

(C) The mRNA expression in tdTomato positive (tdT+) and negative (tdT−) striatal samples analyzed by RT-PCR is shown.

(D) Whole-cell currents evoked by 1-s voltage steps (−100 to 20, ΔV 10 mV), before and after adding 30 nM MgTx, and MgTx-sensitive current are shown.

(E) I-V curve for the MgTx-sensitive current measured at arrow in (D) (n = 5 cells from three juvenile mice). Data are mean ± SEM.

(F) Currents evoked by a voltage ramp in the presence of 1 μM TTX and 30 μM ZD7288 and after sequential addition of 200 μM $Cd^{2+}$and 30 nM MgTx are shown.

(G) MgTx-sensitive conductance is shown.

(H) MgTx-sensitive current amplitude measured at 40 mV versus last spike time is shown (Pearson correlation; n = 5 cells from five juvenile mice).

solution (Figures 2F–2H) and by recording SCINs from K_v1.3 knockout (KO) mice (B6;129S1-*Kcna3tm1Lys*/J; Figures 2I–2K; Table S5). Accommodation was markedly attenuated by all these treatments. For instance, SCINs fired 10.7 ± 0.8 spikes in 886 ± 35 ms in K_v1.3 KO mice and 6.7 ± 1 spikes in 604 ± 81 ms in their wild-type controls (140-pA steps; n = 22–24 SCINs), showing that lack of K_v1.3 expression is not compensated for by alternative K_v1 subunits or K^+ channels in these animals. Altogether, these experiments demonstrate that K_v1.3 subunits are necessary for accommodation in SCINs.

SCINs Express a MgTx-Sensitive Current and K_v1.3 Subunits

Previous reports revealed the expression of K_v1.1 and K_v1.2 mRNA in SCINs (Song et al., 1998). However, K_v1.3 subunit expression has not been investigated before. Antibodies directed against extracellular or intracellular domains of K_v1.3 preferentially labeled tdTomato-positive neurons in the striatum of ChAT-Cre;tdT mice (Figures 3A and 3B). To further assess the expression of K_v1 subunits, we obtained tissue samples containing or excluding SCINs from ChAT-Cre;tdT mice by laser capture

microdissection. As expected, ChAT mRNA was enriched in samples containing SCINs. Interestingly, $K_v1.3$ mRNA was only detected in samples enriched in SCINs (Figure 3C). These results are consistent with a single-cell mRNA profiling study that failed to detect $K_v1.3$ mRNA in the prevailing striatal neuron population, the medium spiny projection neurons (MSNs) (Shen et al., 2004). The $K_v1.1$ mRNA also was detected in SCIN-enriched samples, but the $K_v1.2$ and $K_v1.6$ mRNAs were not (Figure 3C). Also, the SCIN-enriched samples contained mRNAs expressed in MSNs like preproenkephalin (Figure 3C), GAD67, DARPP32, and preprotachykinin mRNAs (not shown), suggesting that mRNAs expressed in MSNs are present in the SCIN-enriched samples. Moreover, Song et al. (1998) reported the presence of $K_v1.2$ mRNA in 25% of SCINs, suggesting that we could have failed to detect mRNAs expressed in low quantities or in a small proportion of SCINs. Nevertheless, our findings are consistent with a main contribution of the $K_v1.3$ and $K_v1.1$ subunits to the effects of toxins on SCINs.

The K_v1 channels are homo- or heterotetramers that carry delayed rectifier type currents whose properties depend on the subunit composition of the channel (Lee et al., 1996; Grissmer et al., 1994). To characterize the MgTx-sensitive current, the whole-cell current amplitude was determined at the end of 1-s voltage steps (−100 to +20 mV, ΔV = 10 mV) in the presence of tetrodotoxin (TTX) to prevent action currents (Figures 3D and 3E). The MgTx-sensitive current had an amplitude of 1.36 ± 0.5 nA when measured at the end of a step to 20 mV, representing 41.7% of the total current (Figures 3D and 3E), and it did not show signs of inactivation (amplitudes at 50 and 500 ms after the beginning of the step were 1.05 ± 0.5 and 1.36 ± 0.5 nA, respectively). To isolate the MgTx-sensitive current and more precisely characterize its voltage dependence, we obtained recordings of whole-cell currents in response to a voltage ramp (Figure 3F). In these experiments, ZD7288 was used to prevent the activation of the prominent I_h expressed by SCINs (Jiang and North, 1991; Kawaguchi, 1993). The average outward current elicited at the end of the ramp (40 mV) in these conditions was 10.5 ± 0.8 nA; 58% of this current was blocked by Cd^{2+} (a non-selective calcium channel blocker), likely representing K_{Ca} currents, and an additional 27% was blocked by MgTx (Figure 3F). We calculated the MgTx-sensitive conductance from the MgTx-sensitive current (Figure 3G) and determined a $V_{50} = -9.6 + 7.3$ mV. Importantly, there was a significant linear correlation between last spike time during a depolarizing current step and the magnitude of the MgTx-sensitive current measured subsequently in the same cells ($p = 0.022$, $R^2 = 0.864$; Figure 3H).

Overall, our data show that, in addition to large Ca^{2+}-activated outward currents, SCINs show a prominent MgTx-sensitive outward current activated only by voltage, which correlates with the strength of accommodation, supporting $K_v1.3$-containing K^+ channels as key players in SCIN excitability.

$K_v1.3$ Subunit-Containing Channels Regulate Tonic Firing and Synaptic Integration in SCINs

Previous studies stressed the role of K_{Ca} conductances in regulating the spontaneous firing rate of SCINs (Goldberg and Wilson, 2005; Bennett and Wilson, 1999); nevertheless, whether K_v channels also are involved remains unknown. Thus, we recorded spontaneous spike discharges in the cell-attached configuration from SCINs of slices exposed to MgTx and control slices (Figures 4A and 4B). Picrotoxin and 6-cyano-7-nitroquinoxaline-2,3-dione (CNQX) were added to the bath to minimize regulation by extrinsic signals. The spontaneous firing rate of SCINs was 70% higher in the presence of MgTx compared to the control condition ($p = 0.012$, Mann-Whitney test; Figure 4C). Thus, MgTx-sensitive channels slow the spontaneous firing rate of SCINs.

Thalamic glutamatergic inputs drive complex responses in SCINs, consisting of a brief excitation followed by a pause in tonic firing, in connection with salient events like reward (Kimura et al., 1984; Apicella et al., 1991). To determine whether $K_v1.3$-containing channels regulate SCIN responses to thalamic input, we expressed channelrhodopsin-2 (ChR2) in thalamostriatal axons by injecting a lentiviral vector in the thalamus of adult mice (Figure 4D). Illumination of thalamostriatal axons with trains of blue light (20 Hz, picrotoxin in the bath) induced synaptic responses in SCINs that were blocked by CNQX (Figure 4E). MgTx dramatically increased temporal integration of this excitatory response (Figures 4F and 4G). Importantly, the subthreshold depolarization induced by thalamic input was followed by an AHP (Figure 4F), which is thought to contribute to the pause response of SCINs to rewarding events (Reynolds et al., 2004). This AHP was markedly diminished or eliminated by MgTx (Figures 4H and 4I). Similar effects were observed both with MgTx and ADWX-1 on synaptic responses evoked by intrastriatal electrical stimulation (Figure S5). Thus, $K_v1.3$ subunit-containing channels might be able to modulate the signals through which SCINs inform the striatal circuitry about reward.

Taken together, these findings show that K_v1 channels have prominent physiological roles in SCINs.

SCINs Are More Excitable and Insensitive to MgTx in 6-OHDA Mice

SCINs are more excitable in rats with a chronic nigrostriatal lesion induced by the neurotoxin 6-OHDA than in control animals. This is evidenced as a lack of accommodation in comparison with sham-lesioned rats (Sanchez et al., 2011). To determine whether nigrostriatal degeneration induces a deficit of accommodation in the mouse, similar to that observed in rats, we studied SCIN excitability in ChAT-Cre;tdT 6-OHDA-treated mice. The 6-OHDA (or vehicle) was injected into the nigrostriatal tract at the medial forebrain bundle in 15- to 20-week-old mice (Escande et al., 2016). Electrophysiological recordings were performed 5–8 weeks after the lesion in animals showing parkinsonian-like motor impairment (Figure S6). Postmortem studies confirmed a depletion of tyrosine hydroxylase (TH)-immunoreactive neurons from the substantia nigra (Figure 5A).

Overall, SCINs are more excitable in 6-OHDA than sham mice of the same age, as shown by a higher number of spikes fired, a longer duration of discharge in response to 1-s depolarizing current pulses, and a lower rheobase across the whole population of recorded SCINs (Figures 5B–5D). Moreover, this excitability change was unevenly distributed across the SCIN population. Unsupervised multivariate clustering also was able to separate SCINs with short last spike times and low excitability from highly

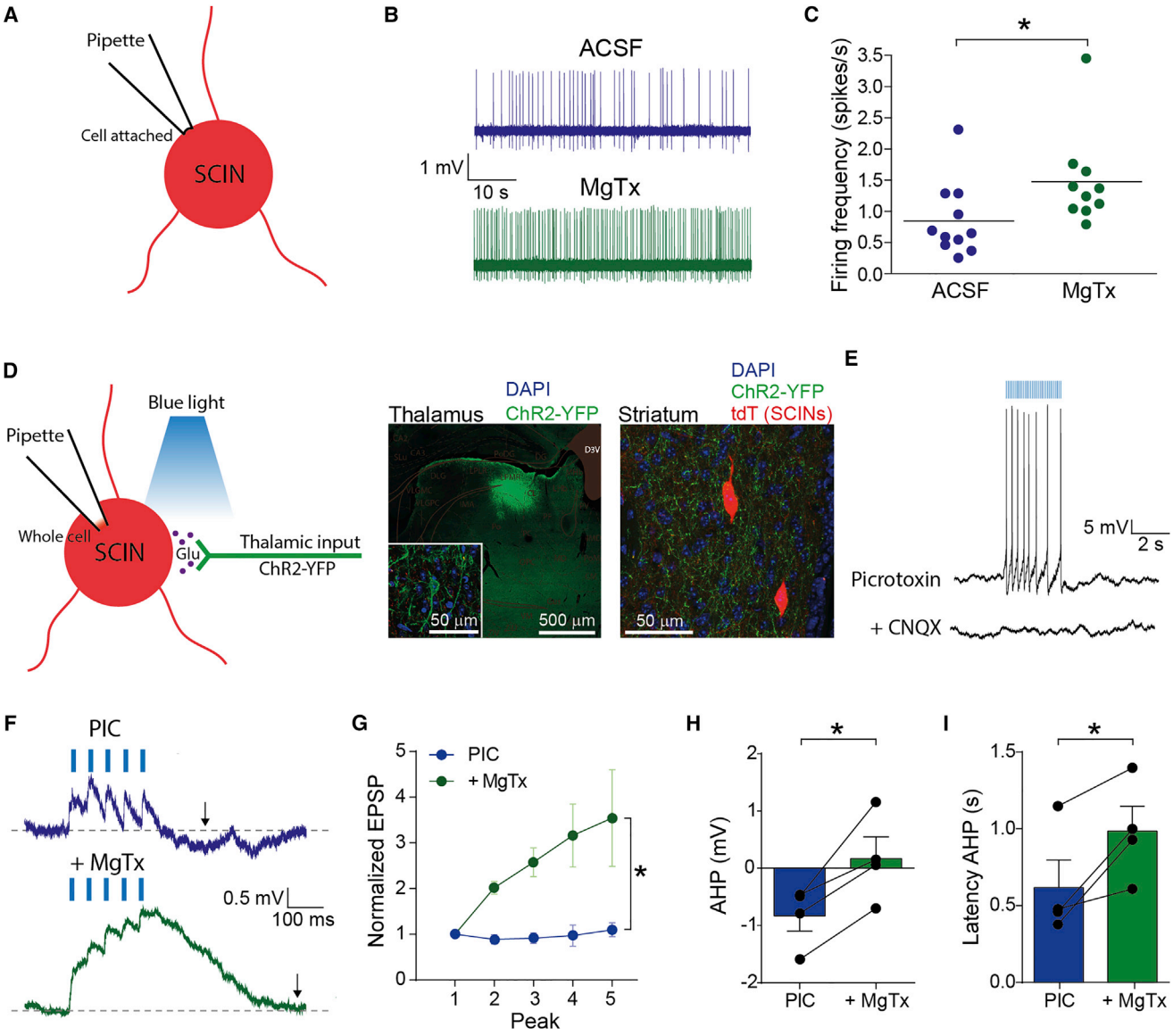

Figure 4. $K_v1.3$ Channels Regulate Tonic Firing and Synaptic Integration in SCINs

(A–C) Schematic diagram and representative traces of cell-attached recordings (A and B) and population data (C) of spontaneous activity, with or without MgTx in the bath, are shown (n = 10–11 cells and six mice per group; p = 0.012, Mann-Whitney test).

(D) Schematic representation of optogenetic stimulation of thalamic inputs (left) to an SCIN recorded in whole-cell configuration. Micrograph shows the thalamic region transfected with ChR2-YFP and striatal region with labeled thalamic terminals and tdT-reported SCINs (right).

(E) Response to optogenetic stimulation before (top) and after (bottom) bath addition of CNQX is shown.

(F and G) Representative traces (F) and normalized EPSP amplitudes (G) evoked by optogenetic stimulation before and after the bath addition of 30 nM MgTx, are shown (two-way RM ANOVA interaction, *p < 0.0001; n = 4 cells from two adult mice).

(H and I) AHP amplitude (H, *p = 0.030) and latency (I, *p = 0.037) before and after MgTx are shown (paired t tests).

Data are mean ± SEM. See Figure S5.

excitable SCINs with long last spike times in this new dataset (Figures 5E, 5F, and S7). On average, in sham mice, non-accommodating SCINs fired 11.1 ± 1 spikes in 839 ± 43 ms and accommodating SCINs fired 4.7 ± 0.4 spikes in 349 ± 24 ms, while in the 6-OHDA-lesioned mice, non-accommodating and accommodating SCINs fired 10.9 ± 0.4 spikes in 886 ± 13 ms and 5.2 ± 0.4 spikes in 436 ± 29 ms, respectively. Thus, accommodating and non-accommodating SCINs differed significantly from each other regardless of lesion ($p < 0.0001$, two-way ANOVA; interaction and lesion effect were non-significant). However, the proportion of non-accommodating SCINs was significantly higher in the 6-OHDA-lesioned mice (Figure 5G; $p = 0.002$, Fisher's exact test). Importantly, SCINs from sham and 6-OHDA mice did not differ in other physiological properties

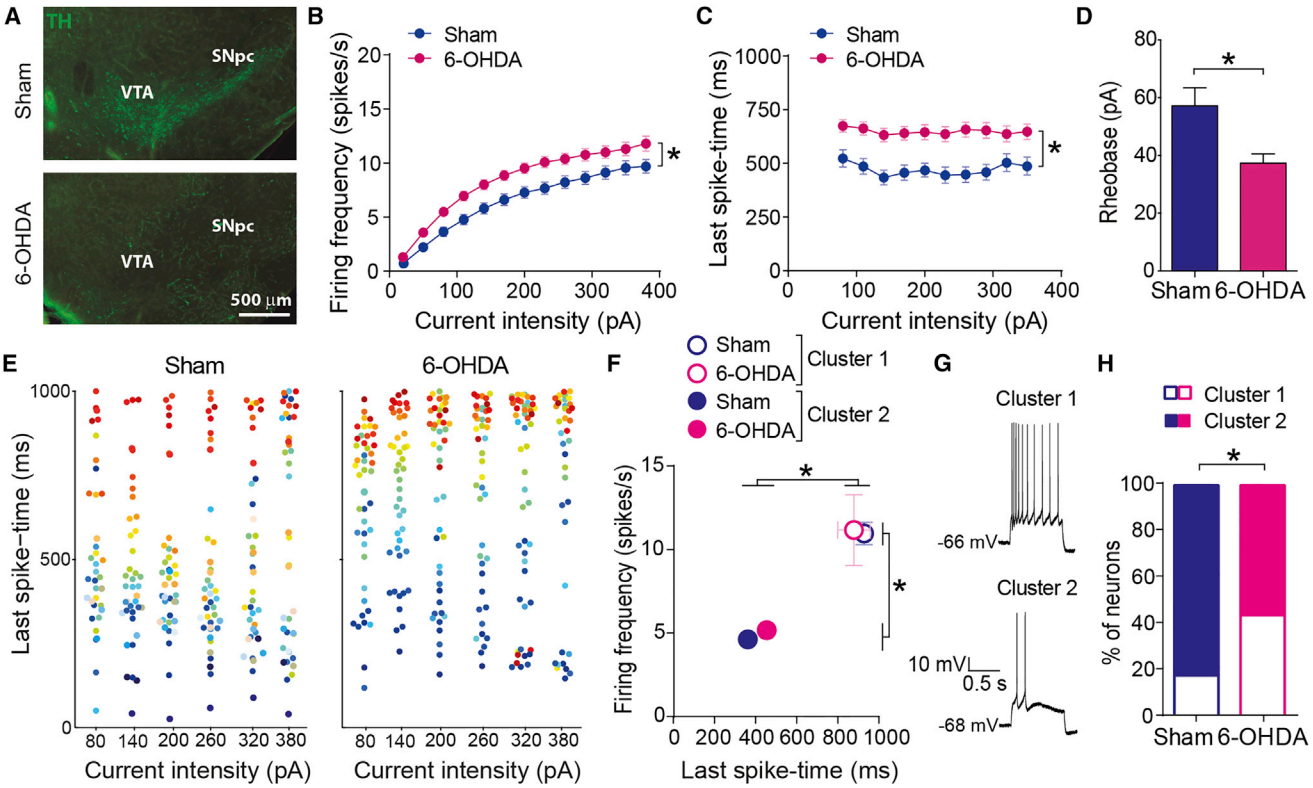

Figure 5. SCINs from 6-OHDA-Lesioned Mice Are More Excitable

(A) Substantia nigra from a sham and a 6-OHDA ChAT-Cre;tdT mouse immunostained for TH is shown.

(B–D) Firing frequency (B) and last spike time (C) versus current intensity (two-way RM ANOVA interaction, **p = 0.005 and lesion effect *p = 0.0001 in C) and rheobase (D, t test, *p = 0.003) for SCINs recorded from sham and 6-OHDA mice are shown (n = 46 cells from 14 sham mice and n = 71 cells from 23 6-OHDA mice).

(E) Last spike times for SCINs from sham (left) or 6-OHDA (right) mice at all currents tested are shown.

(F) Firing frequency versus last spike time (140-pA depolarization) of non-accommodating (cluster 1) and accommodating (cluster 2) SCINs from sham and 6-OHDA mice is shown (*p < 0.0001, two-way ANOVA).

(G and H) Percentages of non-accommodating and accommodating SCINs (G) in sham and 6-OHDA mice (H) are shown (*p < 0.0001, Fisher's exact test).

Data are mean ± SEM. See Figures S6 and S7 and Table S6.

like resting membrane potential, action potential threshold, sag amplitude, sAHP amplitude, and input resistance (Table S6) Thus, the data show that SCINs from animals with nigrostriatal lesion express an excitability phenotype that is normally more common in juvenile than adult animals (see also Sanchez et al., 2011). Interestingly, acute pharmacological blockade of dopamine receptors did not modify the excitability of SCINs in control mice (Figure S6). Thus, the excitability changes relate to adaptations that follow the chronic nigrostriatal lesion.

We reasoned that, if the accommodation deficit observed in 6-OHDA mice was due to a reduction of the $K_v1.3$ current, then SCINs should be less sensitive to MgTx in these animals. As expected, MgTx reduced accommodation in SCINs recorded from sham animals but lacked this effect in 6-OHDA mice (Figures 6A–6C). Similarly, temporal summation of excitatory postsynaptic potentials (EPSPs) induced by intrastriatal electrical stimulation was enhanced and insensitive to MgTx in 6-OHDA-lesioned animals (Figures 6D and 6E). Finally, SCINs from 6-OHDA mice reached a significantly higher frequency of firing during somatic ramp current injection compared to control mouse SCINs, and MgTx enhanced this response in control, but not in 6-OHDA, animals (Figures 6F and 6G). Thus, chronic nigrostriatal lesion turns SCINs more excitable and insensitive to $K_v1.3$ blockade.

SCINs Have Smaller $K_v1.3$ Currents in Parkinsonian Mice

We speculated that a decrease of the MgTx-sensitive conductance causes the hyperexcitability of SCINs observed after chronic nigrostriatal lesion. When recorded in the presence of TTX, ZD7288, and Cd^{2+}, SCINs from 6-OHDA-lesioned animals showed smaller outward currents in response to depolarizing voltage steps compared to SCINs from sham mice (1,376 ± 259 pA versus 2,849 ± 317 pA at +20 mV, respectively; p < 0.05, Tukey's post hoc test after significant interaction; p = 0.0015, two-way ANOVA; Figures 6H and 6I). As expected, in sham mice, outward currents were substantially smaller when recorded in the presence of MgTx (p < 0.05, Tukey's post hoc). Moreover, the residual outward current recorded in the presence of MgTx in sham mice (1,000 ± 142 pA at +20 mV) was similar to that recorded in 6-OHDA mice in the presence (1,283 ± 135 pA) or absence of MgTx (1,376 ± 259 pA), and MgTx had no effect on the outward currents recorded from 6-OHDA-lesioned mice

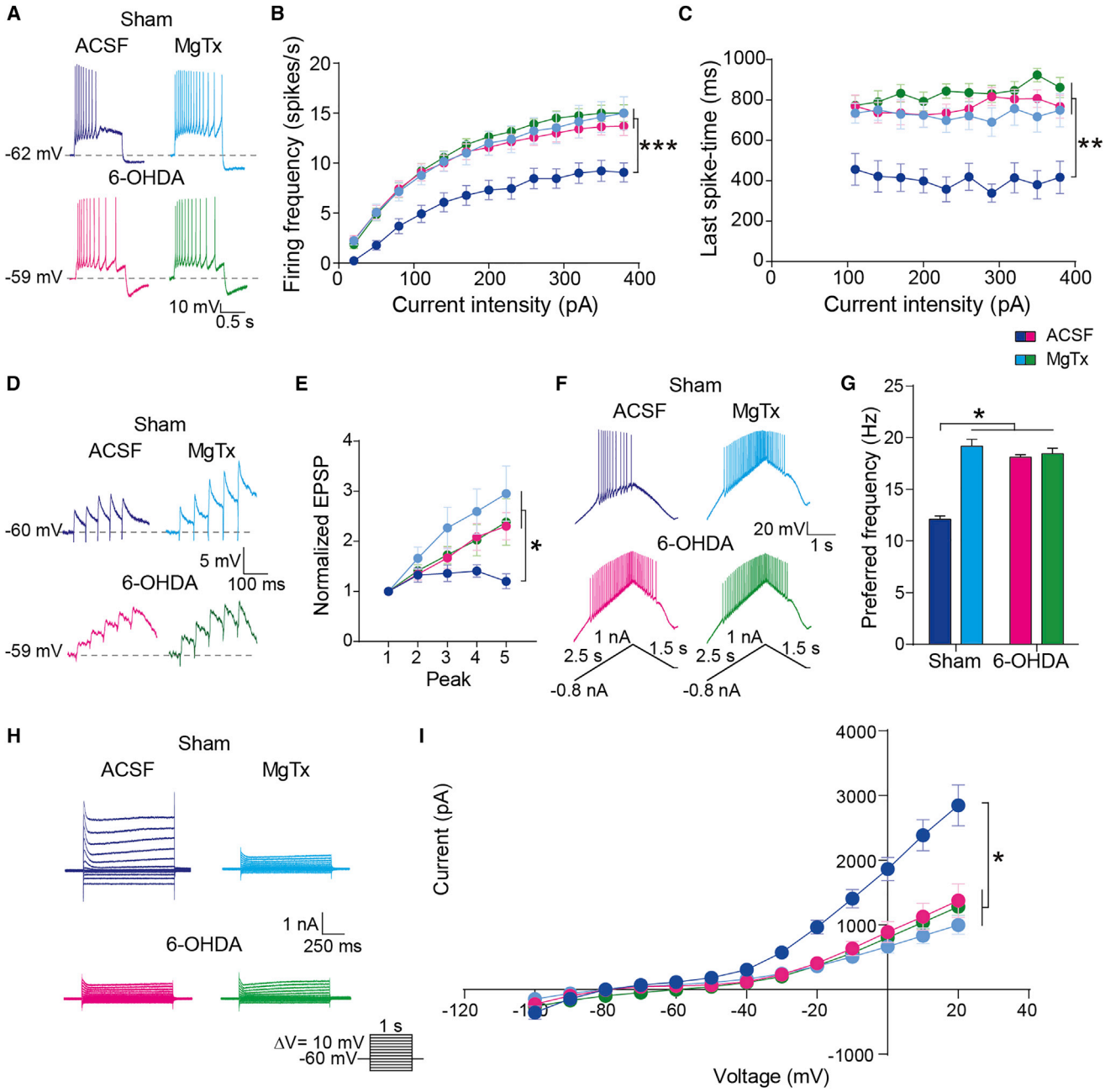

Figure 6. The MgTx-Sensitive Current Is Absent from SCINs of 6-OHDA Mice

(A) Representative recordings show adult SCINs from sham and 6-OHDA mice before and after bath application of 30 nM MgTx.

(B and C) Effects of MgTx on SCIN firing frequency (B) and last spike time (C) in sham and 6-OHDA mice are shown (two-way RM ANOVA interaction, ***$p < 0.0001$ and group effect: **$p < 0.0001$ in C; n = 13 cells from four adult mice in each group).

(D and E) Representative traces (D) and normalized EPSP amplitude (E) for SCINs from sham and 6-OHDA mice before and after the bath addition of 30 nM MgTx, are shown (two-way RM ANOVA interaction, last EPSP: *$p = 0.035$; n = 6–7 cells from three sham and three 6-OHDA mice).

(F and G) Representative responses (F) and preferred firing frequency (G) of SCINs from sham and 6-OHDA mice during a current clamp ramp before and after the bath application of 30 nM MgTx, are shown (two-way RM ANOVA interaction, *$p = 0.0003$, Bonferroni post hoc; n = 7–8 cells from three sham mice and three 6-OHDA mice).

(H and I) Representative whole-cell currents (H) and average I-V curves (I; n > 4 cells and four mice per group) of SCINs recorded from sham or 6-OHDA mice, with or without MgTx (*$p < 0.0001$, two-way RM ANOVA interaction). Data are mean ± SEM.

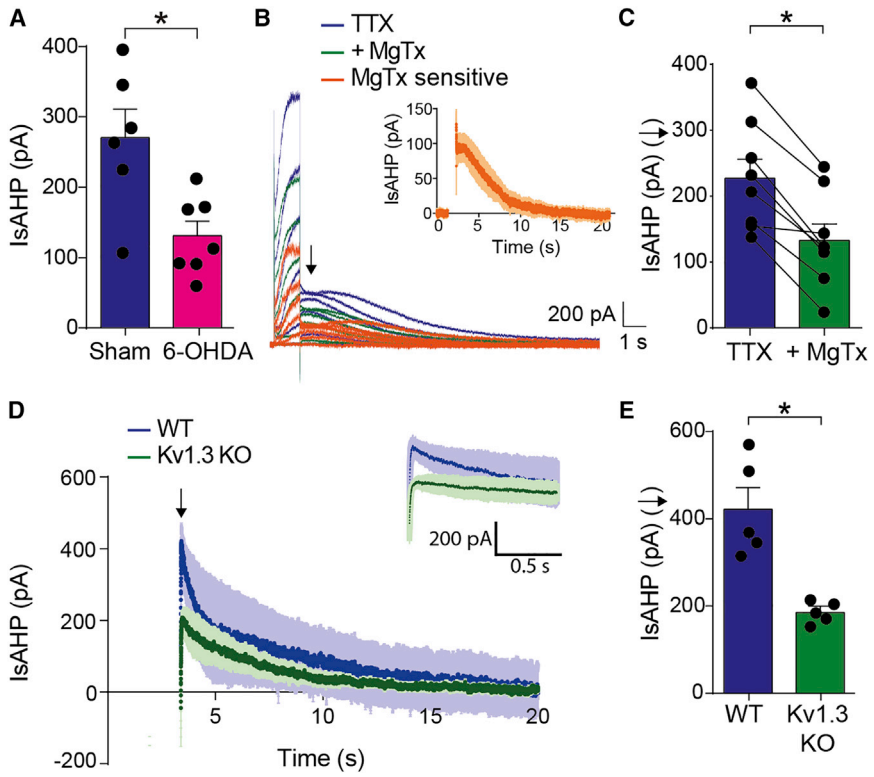

Figure 7. I_{sAHP} Has a $K_v1.3$ Component in SCINs

(A) I_{sAHP} evoked by a 1-s voltage step from −50 to 0 mV in sham and 6-OHDA-lesioned mice is shown (four mice per group; $p < 0.01$, unpaired t test).

(B) Representative currents evoked by 1-s depolarizing voltage steps (−50 to 0 mV, ΔV 10 mV, holding −50 mV) in ACSF with 1 μM TTX and after adding MgTx. Inset: MgTx-sensitive component of I_{sAHP} is shown (n = 8 cells from seven mice).

(C) I_{sAHP} peak amplitude (arrow in B) decreases after adding MgTx (Mann-Whitney test, $p = 0.0002$).

(D) Currents evoked by 1-s depolarizing voltage steps with 1 μM TTX in the bath, in WT and $K_v1.3$ KO mice, are shown (four animals per group).

(E) I_{sAHP} peak amplitude (arrow in D) in WT and $K_v1.3$ KO mice is shown (Mann-Whitney test, $p = 0.038$).

Data are mean ± SEM.

(non-significant Tukey's post hoc tests after significant interaction, two-way ANOVA; Figure 6I). Altogether, the data support that a reduction of the MgTx-sensitive current causes the accommodation and synaptic integration deficits observed in SCINs of 6-OHDA-lesioned mice.

The $K_v1.3$ Current Contributes to I_{sAHP} and Is Active at Close-to-Threshold Membrane Potentials

I_{sAHP} is usually assessed as the tail current induced by long depolarizing voltage steps that depart from a holding potential mimicking the resting membrane potential of the studied cell. In SCINs, these protocols evoke barium-sensitive and barium-insensitive components, the barium-sensitive component being reduced in 6-OHDA-lesioned rats (Sanchez et al., 2011). The barium-insensitive component, which is the classical I_{sAHP} current linked to DHP-sensitive Ca_v channels (Goldberg and Wilson, 2005; Goldberg et al., 2009), seemed not to be involved in accommodation, which persists after bath application of DHPs in SCINs (Sanchez et al., 2011). Because the relationship between our current findings and those of Sanchez et al. (2011) remained unclear, we asked whether the $K_v1.3$ current contributes to I_{sAHP} in SCINs.

First we asked whether I_{sAHP} diminishes after a 6-OHDA-induced lesion in the mouse as it happens in the rat (Figure 7A). I_{sAHP} was assessed 0.5 s after a 1-s step to 0 mV that departed from a holding potential of −50 mV (Figure 7B), as in previous studies of I_{sAHP} in SCINs (Sanchez et al., 2011; Goldberg and Wilson, 2005). At its peak, I_{sAHP} was 52% smaller in 6-OHDA-lesioned than in sham mice (131 ± 21 and 271 ± 41 pA, respectively; $p = 0.008$, unpaired t test). Then we tested whether I_{sAHP} is MgTx sensitive in mouse control SCINs (Figures 7B and 7C). Addition of MgTx (30 nM) to the bath decreased I_{sAHP} by 41% at its peak (from 227 ± 29 to 133 ± 25 pA; $p = 0.0002$, paired t test; Figure 7C). Finally, we asked if the MgTx-sensitive current is active when the membrane potential is held at −50 mV, as is the case with the rat barium-sensitive component of I_{sAHP} (Sanchez et al., 2011). The MgTx-sensitive current was 105 ± 32 pA while holding the membrane potential at −50 mV, which represents 13% of the current measured at the end of 1-s steps to 0 mV (826 ± 164 pA, Figure 7B).

Because a contribution of K_v1 channels to I_{sAHP} was unexpected based on the properties shown by K_v1 currents in cell expression systems, we examined the I_{sAHP} in $K_v1.3$ KO mice (Figures 7D and 7E). The current was reduced by ~50% in $K_v1.3$ KO animals. Overall, the data show that $K_v1.3$ subunit-containing channels contribute to I_{sAHP} in SCINs.

DISCUSSION

The present study reveals unexpected physiological roles of a delayed rectifier-type K_v current in SCINs. The current provides strong negative feedback to depolarization that limits SCIN temporal integration of excitatory inputs, burst firing, and tonic spontaneous activity. Pharmacological, genetic, and molecular expression studies show that $K_v1.3$ subunits form part of the channels that carry this current. Moreover, the distinctive hyperexcitability of SCINs that follows nigrostriatal lesion is associated with a reduction of this K_v1 current, and it resembles very closely the hyperexcitability induced by toxins that block $K_v1.3$ channels and is observed in $K_v1.3$ KO mice. More specifically, in normal conditions, repetitive spike firing and temporal summation of excitatory inputs are limited by the $K_v1.3$ current. In contrast,

spike firing keeps going throughout sustained depolarizations and synaptic integration is enhanced when channels containing $K_v1.3$ subunits are blocked or knocked out or after chronic nigrostriatal degeneration.

It has been long known that SCINs express a delayed rectifier-type K^+ current (Song et al., 1998) that supposedly speeds the repolarization phase of action potentials (Deng et al., 2005; Goldberg et al., 2009), but whether K_v1 channels contribute to shape SCIN firing patterns remained unknown. SCINs show tonic spike-firing activity of intrinsic origin in resting conditions (Bennett and Wilson, 1999). Moreover, they respond to salient environmental stimuli with a synaptically driven increase of firing followed by a pause in tonic activity (Kimura et al., 1984; Apicella et al., 1991). Both the pace of tonic activity and the pause induced by salient stimuli depend, to some extent, on negative feedback provided by intrinsic K^+ conductances (Bennett et al., 2000; Reynolds and Wickens, 2004; Wilson, 2005; Schulz et al., 2011). Our data obtained in the cell-attached recording configuration that preserves the composition of the internal cell milieu show that $K_v1.3$ blockade increases the tonic activity of SCINs. Moreover, the finding that the $K_v1.3$ current limits spike firing during a sustained depolarization suggests that it may shape the pause response of SCINs to salient events. This is further supported by the observation that temporal integration of excitatory thalamic input is limited by $K_v1.3$ channels. Importantly, excitatory input drives an AHP in the presence of picrotoxin, which is reduced or abolished by $K_v1.3$ blockade. These effects are highly selective, as several other physiological properties of SCINs, including the duration of the action potential, remain unchanged after $K_v1.3$ blockade. While highly unexpected for SCINs, whose firing patterns are thought to be determined by Ca_v, K_{Ca}, and HCN channels, regulation of discharge patterns by K_v1 currents without changes in action potential duration has been noticed before in other central and peripheral neurons (Dodson et al., 2002; Faber and Sah, 2004).

K_v1 channels are constituted by four pore-forming voltage-sensing α subunits that coassemble into homomeric or heteromeric channels with varied functional properties (Yellen, 2002). Our pharmacological and molecular expression studies indicate that channels containing $K_v1.1$ and $K_v1.3$ subunits likely mediate the observed physiological effects. This is further supported by similar effects of *KCNA3* deletion and $K_v1.3$ immunological blockade on SCIN excitability to those of toxins that block channels with $K_v1.3$ subunits. A pioneering single-cell mRNA-profiling study detected $K_v1.4$ in most and $K_v1.2$ in some SCINs, ruled out the presence of $K_v1.5$, and established that the $\beta1$ and $\beta2$ auxiliary subunits that regulate K_v1 channel function also are expressed by SCINs (Song et al., 1998). Since $K_v1.3$ can coassemble with any of these α and β subunits (Coleman et al., 1999) and the binding of just one molecule of MgTx can block the channel regardless of its homo- or heteromeric constitution (Hopkins, 1998), SCINs could be equipped with a variety of K_v1 tetramers. Likely, the $K_v1.3$ subunits are mostly integrated into heterotetramers because homomeric $K_v1.3$ channels show a distinctive slow inactivation (Stühmer et al., 1989; Grissmer et al., 1994), which is not seen in our recordings. Other properties of the $K_v1.3$ current, like its half-activation voltage and its activity at subthreshold potentials, are similar to those previously reported in other native preparations for low-threshold-delayed rectifier K^+ channels (Guan et al., 2006; Iwasaki et al., 2008).

Resembling the phenotype observed after $K_v1.3$ blockade, SCINs show a specific deficit in accommodation of spike firing and an enhanced integration of excitatory synaptic input in 6-OHDA-lesioned mice. This would be expected to distort the brief excitatory response followed by a pause through which SCINs inform about rewarding events, thus providing a putative explanation for the attenuation of these responses in monkeys with experimental parkinsonism (Aosaki et al., 1994). Moreover, we provide compelling evidence that these physiological deficits induced by the 6-OHDA lesion are due to a reduction of the $K_v1.3$ current. Of note, SCINs do not show changes in spontaneous activity after dopamine depletion (Ding et al., 2006; Maurice et al., 2015), suggesting that compensatory mechanisms may attenuate the effect of the lack of $K_v1.3$ current on tonic firing. Thus, the available data are consistent with an enhanced response of SCINs to stimulation after chronic dopamine depletion.

Theoretically, the reduction of the $K_v1.3$ current could relate to a decreased expression of the $K_v1.3$ channels and/or to alterations of their trafficking and regulatory mechanisms. Currents carried by $K_v1.3$ channels are regulated by serine/threonine (Kupper et al., 1995) and tyrosine phosphorylation (Fadool et al., 1997), co-expression of KCNE4 (Grunnet et al., 2003) and β subunits (McCormack et al., 1999), ubiquitination (Henke et al., 2004), and interactions with scaffolding proteins (Doczi et al., 2011). Preliminary findings show that SCINs display $K_v1.3$ subunit immunoreactivity in 6-OHDA mice (Figure S6). Furthermore, SCIN excitability is insensitive to interventions that regulate RGS4, which is overexpressed by SCINs after a 6-OHDA lesion (Ding et al., 2006; Figure S6). Further studies are needed to establish the mechanisms that reduce the K_v1 current after nigrostriatal lesion.

The I_{sAHP} was originally described in cortical pyramidal cells as a feedback mechanism that limits repetitive firing by inducing a sAHP lasting several seconds (Alger and Nicoll, 1980; Storm, 1990). The sAHP is thought to be mediated by an unidentified K_{Ca} current, but additional currents may be involved in hippocampal neurons (Andrade et al., 2012). In this regard, SCINs show sAHP-like hyperpolarizations that are not related to cytosolic Ca^{2+} transients (Goldberg et al., 2009) and persist after the blockade of the DHP-sensitive Ca_v channels that presumptively activate the I_{sAHP} in SCINs (Sanchez et al., 2011). Our finding of a $K_v1.3$ component of I_{sAHP} adds to recent studies showing that K_v7 and TREK1 channels (Tzingounis and Nicoll, 2008; Ford et al., 2013) contribute to the I_{sAHP} in other neurons. Interestingly, $K_v1.3$ blockade does not modify the sAHP that follows long-duration depolarizing currents steps applied to SCINs, but it decreases the AHP induced by stimulation of afferent excitatory inputs. We speculate that, under $K_v1.3$ blockade, the enhanced action potential response to current steps recruits more effectively the remaining components of I_{sAHP}, which could suffice to maintain the sAHP unchanged. In contrast, subthreshold synaptic responses could be less effective to drive the K_{Ca} component of I_{sAHP}, inducing a $K_v1.3$-dependent AHP. While the identity of the canonical K_{Ca} component of I_{sAHP} in SCINs

remains to be determined, the data available suggest that it is not affected by the nigrostriatal lesion (Sanchez et al., 2011).

In sum, a low-threshold-delayed rectifier type K^+ conductance involving $K_v1.3$ subunits shapes the firing patterns and synaptic responses of SCINs. Its role may complement that played by K_{Ca} conductances, as it happens in immune cells where a well-known $K_v1.3$ conductance interacts with $K_{Ca}3.1$ channels to set the membrane potential oscillations that drive immune responses (Feske et al., 2015). Additionally, this $K_v1.3$ current is markedly reduced in SCINs in a mouse model of PD, pointing to $K_v1.3$ subunit-containing channels and their regulatory pathways as potential new targets for PD therapy.

EXPERIMENTAL PROCEDURES

See also the Supplemental Experimental Procedures.

Mice were obtained by crossing ChAT-Cre and Rosa-CAG-LSL-tdTomato-WPRE mice. Animal care was in accordance with institutional (Institutional Animal Care and Use Committee, School of Medicine, University of Buenos Aires, 2598/13) and government regulations (Servicio Nacional de Sanidad y Calidad Agroalimentaria). Nigrostriatal lesions were obtained by injecting 6-OHDA into the left medial forebrain bundle (MFB) under isoflurane anesthesia (Escande et al., 2016). Following similar anesthesia and surgical procedures, a ChR2-YFP-expressing lentivirus pseudotyped with the vesicular stomatitis virus glycoprotein was injected into the left thalamus.

For the slice recordings, mice were anesthetized with chloral hydrate and decapitated. Recordings were performed in 300-μm-thick coronal slices, at 34°C, in a submerged-type chamber perfused at 3 ml/min with standard artificial cerebrospinal fluid (ACSF). Recording pipettes (4–7 MΩ) were filled with a K^+ gluconate-based internal solution or ACSF for whole-cell and cell-attached recordings, respectively. SCINs were sampled from the dorsolateral striatum. Optogenetic stimulation was generated with a 447-nm light-emitting diode (Tolket) and delivered through an optic fiber placed <300μm from the recorded cell. Intrastriatal electric stimulation was delivered through a bipolar electrode placed at ~500 μm from the recorded cell.

SCINs were classified as accommodating or non-accommodating using principal-component analysis followed by unsupervised multivariate clustering (Ward's method). The V_{50} of the MgTx-sensitive current was calculated from a Boltzman fit to the normalized curve of conductance. Data were tested for normality and homoscedasticity before using parametric statistics (t test or ANOVA depending on the numbers of groups and factors). Statistical tests are indicated in the figure legends or text.

SUPPLEMENTAL INFORMATION

Supplemental Information includes Supplemental Experimental Procedures, seven figures, and six tables and can be found with this article online at http://dx.doi.org/10.1016/j.celrep.2016.08.016.

AUTHOR CONTRIBUTIONS

L.R. and M.G.M. designed the study. C.T. performed the experiments. I.R.E.T. did the 6-OHDA lesions. Data from $K_v1.3$ KO mice were collected by C.T. and E.F.-B. in the K.Y.T. lab. M.A.P. did the characterization of ChAT-Cre;tdT mice. M.E.A. prepared lentiviral vectors. G.M.S. obtained key preliminary data. C.T., E.F.-B., K.Y.T., and L.R. analyzed data. C.T., K.Y.T., L.R., and M.G.M. wrote the manuscript.

ACKNOWLEDGMENTS

The authors thank P. Pomata, G. Ortega, and M. Brahamian for excellent technical assistance; J. Belforte, F. Urbano, and L. Riquelme for helpful discussions; V. Gazula and L. Kaczmarek for advice on $K_v1.3$ immunodetection; H. Wulff for helpful information about pharmacological reagents; and C. Zold for checking the use of language. This study was supported by Fondo para la Investigación Científica y Tecnológica (FONCYT; Proyecto de Investigación Científica y Tecnológica [PICT] 2011-521, 2013-1523, and 2015-3687), Tourette Syndrome Association, and Universidad de Buenos Aires (UBACYT2014-249).

Received: November 3, 2015
Revised: June 16, 2016
Accepted: August 5, 2016
Published: August 25, 2016

REFERENCES

Alger, B.E., and Nicoll, R.A. (1980). Epileptiform burst afterhyperolarization: calcium-dependent potassium potential in hippocampal CA1 pyramidal cells. Science *210*, 1122–1124.

Andrade, R., Foehring, R.C., and Tzingounis, A.V. (2012). The calcium-activated slow AHP: cutting through the Gordian knot. Front. Cell. Neurosci. *6*, 47.

Aosaki, T., Graybiel, A.M., and Kimura, M. (1994). Effect of the nigrostriatal dopamine system on acquired neural responses in the striatum of behaving monkeys. Science *265*, 412–415.

Apicella, P., Scarnati, E., and Schultz, W. (1991). Tonically discharging neurons of monkey striatum respond to preparatory and rewarding stimuli. Exp. Brain Res. *84*, 672–675.

Barbeau, A. (1962). The pathogenesis of Parkinson's disease: a new hypothesis. Can. Med. Assoc. J. *87*, 802–807.

Bennett, B.D., and Wilson, C.J. (1999). Spontaneous activity of neostriatal cholinergic interneurons in vitro. J. Neurosci. *19*, 5586–5596.

Bennett, B.D., Callaway, J.C., and Wilson, C.J. (2000). Intrinsic membrane properties underlying spontaneous tonic firing in neostriatal cholinergic interneurons. J. Neurosci. *20*, 8493–8503.

Coleman, S.K., Newcombe, J., Pryke, J., and Dolly, J.O. (1999). Subunit composition of Kv1 channels in human CNS. J. Neurochem. *73*, 849–858.

Cooper, E.C., Harrington, E., Jan, Y.N., and Jan, L.Y. (2001). M channel KCNQ2 subunits are localized to key sites for control of neuronal network oscillations and synchronization in mouse brain. J. Neurosci. *21*, 9529–9540.

Cragg, S.J. (2006). Meaningful silences: how dopamine listens to the ACh pause. Trends Neurosci. *29*, 125–131.

DeBoer, P., Heeringa, M.J., and Abercrombie, E.D. (1996). Spontaneous release of acetylcholine in striatum is preferentially regulated by inhibitory dopamine D2 receptors. Eur. J. Pharmacol. *317*, 257–262.

Deffains, M., and Bergman, H. (2015). Striatal cholinergic interneurons and cortico-striatal synaptic plasticity in health and disease. Mov. Disord. *30*, 1014–1025.

Deng, P., Pang, Z.P., Zhang, Y., and Xu, Z.C. (2005). Increase of delayed rectifier potassium currents in large aspiny neurons in the neostriatum following transient forebrain ischemia. Neuroscience *131*, 135–146.

Deng, P., Zhang, Y., and Xu, Z.C. (2007). Involvement of I(h) in dopamine modulation of tonic firing in striatal cholinergic interneurons. J. Neurosci. *27*, 3148–3156.

Ding, J., Guzman, J.N., Tkatch, T., Chen, S., Goldberg, J.A., Ebert, P.J., Levitt, P., Wilson, C.J., Hamm, H.E., and Surmeier, D.J. (2006). RGS4-dependent attenuation of M4 autoreceptor function in striatal cholinergic interneurons following dopamine depletion. Nat. Neurosci. *9*, 832–842.

Ding, Y., Won, L., Britt, J.P., Lim, S.A., McGehee, D.S., and Kang, U.J. (2011). Enhanced striatal cholinergic neuronal activity mediates L-DOPA-induced dyskinesia in parkinsonian mice. Proc. Natl. Acad. Sci. USA *108*, 840–845.

Doczi, M.A., Damon, D.H., and Morielli, A.D. (2011). A C-terminal PDZ binding domain modulates the function and localization of Kv1.3 channels. Exp. Cell Res. *317*, 2333–2341.

Dodson, P.D., Barker, M.C., and Forsythe, I.D. (2002). Two heteromeric Kv1 potassium channels differentially regulate action potential firing. J. Neurosci. *22*, 6953–6961.

Escande, M.V., Taravini, I.R., Zold, C.L., Belforte, J.E., and Murer, M.G. (2016). Loss of homeostasis in the direct pathway in a mouse model of asymptomatic Parkinson's disease. J. Neurosci. *36*, 5686–5698.

Faber, E.S., and Sah, P. (2004). Opioids inhibit lateral amygdala pyramidal neurons by enhancing a dendritic potassium current. J. Neurosci. *24*, 3031–3039.

Fadool, D.A., Holmes, T.C., Berman, K., Dagan, D., and Levitan, I.B. (1997). Tyrosine phosphorylation modulates current amplitude and kinetics of a neuronal voltage-gated potassium channel. J. Neurophysiol. *78*, 1563–1573.

Feske, S., Wulff, H., and Skolnik, E.Y. (2015). Ion channels in innate and adaptive immunity. Annu. Rev. Immunol. *33*, 291–353.

Ford, K.J., Arroyo, D.A., Kay, J.N., Lloyd, E.E., Bryan, R.M., Jr., Sanes, J.R., and Feller, M.B. (2013). A role for TREK1 in generating the slow afterhyperpolarization in developing starburst amacrine cells. J. Neurophysiol. *109*, 2250–2259.

Garcia-Calvo, M., Leonard, R.J., Novick, J., Stevens, S.P., Schmalhofer, W., Kaczorowski, G.J., and Garcia, M.L. (1993). Purification, characterization, and biosynthesis of margatoxin, a component of Centruroides margaritatus venom that selectively inhibits voltage-dependent potassium channels. J. Biol. Chem. *268*, 18866–18874.

Goldberg, J.A., and Wilson, C.J. (2005). Control of spontaneous firing patterns by the selective coupling of calcium currents to calcium-activated potassium currents in striatal cholinergic interneurons. J. Neurosci. *25*, 10230–10238.

Goldberg, J.A., Teagarden, M.A., Foehring, R.C., and Wilson, C.J. (2009). Nonequilibrium calcium dynamics regulate the autonomous firing pattern of rat striatal cholinergic interneurons. J. Neurosci. *29*, 8396–8407.

Grissmer, S., Nguyen, A.N., Aiyar, J., Hanson, D.C., Mather, R.J., Gutman, G.A., Karmilowicz, M.J., Auperin, D.D., and Chandy, K.G. (1994). Pharmacological characterization of five cloned voltage-gated K+ channels, types Kv1.1, 1.2, 1.3, 1.5, and 3.1, stably expressed in mammalian cell lines. Mol. Pharmacol. *45*, 1227–1234.

Grunnet, M., Rasmussen, H.B., Hay-Schmidt, A., Rosenstierne, M., Klaerke, D.A., Olesen, S.P., and Jespersen, T. (2003). KCNE4 is an inhibitory subunit to Kv1.1 and Kv1.3 potassium channels. Biophys. J. *85*, 1525–1537.

Guan, D., Lee, J.C., Tkatch, T., Surmeier, D.J., Armstrong, W.E., and Foehring, R.C. (2006). Expression and biophysical properties of Kv1 channels in supragranular neocortical pyramidal neurones. J. Physiol. *571*, 371–389.

Henke, G., Maier, G., Wallisch, S., Boehmer, C., and Lang, F. (2004). Regulation of the voltage gated K+ channel Kv1.3 by the ubiquitin ligase Nedd4-2 and the serum and glucocorticoid inducible kinase SGK1. J. Cell. Physiol. *199*, 194–199.

Hopkins, W.F. (1998). Toxin and subunit specificity of blocking affinity of three peptide toxins for heteromultimeric, voltage-gated potassium channels expressed in Xenopus oocytes. J. Pharmacol. Exp. Ther. *285*, 1051–1060.

Iwasaki, S., Chihara, Y., Komuta, Y., Ito, K., and Sahara, Y. (2008). Low-voltage-activated potassium channels underlie the regulation of intrinsic firing properties of rat vestibular ganglion cells. J. Neurophysiol. *100*, 2192–2204.

Jiang, Z.G., and North, R.A. (1991). Membrane properties and synaptic responses of rat striatal neurones in vitro. J. Physiol. *443*, 533–553.

Kalia, L.V., and Lang, A.E. (2015). Parkinson's disease. Lancet *386*, 896–912.

Kawaguchi, Y. (1993). Physiological, morphological, and histochemical characterization of three classes of interneurons in rat neostriatum. J. Neurosci. *13*, 4908–4923.

Kimura, M., Rajkowski, J., and Evarts, E. (1984). Tonically discharging putamen neurons exhibit set-dependent responses. Proc. Natl. Acad. Sci. USA *81*, 4998–5001.

King, B., Rizwan, A.P., Asmara, H., Heath, N.C., Engbers, J.D., Dykstra, S., Bartoletti, T.M., Hameed, S., Zamponi, G.W., and Turner, R.W. (2015). IKCa channels are a critical determinant of the slow AHP in CA1 pyramidal neurons. Cell Rep. *11*, 175–182.

Kupper, J., Bowlby, M.R., Marom, S., and Levitan, I.B. (1995). Intracellular and extracellular amino acids that influence C-type inactivation and its modulation in a voltage-dependent potassium channel. Pflugers Arch. *430*, 1–11.

Lee, T.E., Philipson, L.H., and Nelson, D.J. (1996). N-type inactivation in the mammalian Shaker K+ channel Kv1.4. J. Membr. Biol. *151*, 225–235.

Maurice, N., Mercer, J., Chan, C.S., Hernandez-Lopez, S., Held, J., Tkatch, T., and Surmeier, D.J. (2004). D2 dopamine receptor-mediated modulation of voltage-dependent Na+ channels reduces autonomous activity in striatal cholinergic interneurons. J. Neurosci. *24*, 10289–10301.

Maurice, N., Liberge, M., Jaouen, F., Ztaou, S., Hanini, M., Camon, J., Deisseroth, K., Amalric, M., Kerkerian-Le Goff, L., and Beurrier, C. (2015). Striatal cholinergic interneurons control motor behavior and basal ganglia function in experimental parkinsonism. Cell Rep. *13*, 657–666.

McCormack, T., McCormack, K., Nadal, M.S., Vieira, E., Ozaita, A., and Rudy, B. (1999). The effects of Shaker beta-subunits on the human lymphocyte K+ channel Kv1.3. J. Biol. Chem. *274*, 20123–20126.

Nelson, A.B., Hammack, N., Yang, C.F., Shah, N.M., Seal, R.P., and Kreitzer, A.C. (2014). Striatal cholinergic interneurons Drive GABA release from dopamine terminals. Neuron *82*, 63–70.

Peters, H.C., Hu, H., Pongs, O., Storm, J.F., and Isbrandt, D. (2005). Conditional transgenic suppression of M channels in mouse brain reveals functions in neuronal excitability, resonance and behavior. Nat. Neurosci. *8*, 51–60.

Pisani, A., Bernardi, G., Ding, J., and Surmeier, D.J. (2007). Re-emergence of striatal cholinergic interneurons in movement disorders. Trends Neurosci. *30*, 545–553.

Reynolds, J.N., and Wickens, J.R. (2004). The corticostriatal input to giant aspiny interneurons in the rat: a candidate pathway for synchronising the response to reward-related cues. Brain Res. *1011*, 115–128.

Reynolds, J.N., Hyland, B.I., and Wickens, J.R. (2004). Modulation of an afterhyperpolarization by the substantia nigra induces pauses in the tonic firing of striatal cholinergic interneurons. J. Neurosci. *24*, 9870–9877.

Sah, P., and Faber, E.S. (2002). Channels underlying neuronal calcium-activated potassium currents. Prog. Neurobiol. *66*, 345–353.

Sanchez, G., Rodriguez, M.J., Pomata, P., Rela, L., and Murer, M.G. (2011). Reduction of an afterhyperpolarization current increases excitability in striatal cholinergic interneurons in rat parkinsonism. J. Neurosci. *31*, 6553–6564.

Schulz, J.M., Oswald, M.J., and Reynolds, J.N. (2011). Visual-induced excitation leads to firing pauses in striatal cholinergic interneurons. J. Neurosci. *31*, 11133–11143.

Sciamanna, G., and Wilson, C.J. (2011). The ionic mechanism of gamma resonance in rat striatal fast-spiking neurons. J. Neurophysiol. *106*, 2936–2949.

Shen, W., Hernandez-Lopez, S., Tkatch, T., Held, J.E., and Surmeier, D.J. (2004). Kv1.2-containing K+ channels regulate subthreshold excitability of striatal medium spiny neurons. J. Neurophysiol. *91*, 1337–1349.

Song, W.J., Tkatch, T., Baranauskas, G., Ichinohe, N., Kitai, S.T., and Surmeier, D.J. (1998). Somatodendritic depolarization-activated potassium currents in rat neostriatal cholinergic interneurons are predominantly of the A type and attributable to coexpression of Kv4.2 and Kv4.1 subunits. J. Neurosci. *18*, 3124–3137.

Storm, J.F. (1990). Potassium currents in hippocampal pyramidal cells. Prog. Brain Res. *83*, 161–187.

Stühmer, W., Ruppersberg, J.P., Schröter, K.H., Sakmann, B., Stocker, M., Giese, K.P., Perschke, A., Baumann, A., and Pongs, O. (1989). Molecular basis of functional diversity of voltage-gated potassium channels in mammalian brain. EMBO J. *8*, 3235–3244.

Threlfell, S., Lalic, T., Platt, N.J., Jennings, K.A., Deisseroth, K., and Cragg, S.J. (2012). Striatal dopamine release is triggered by synchronized activity in cholinergic interneurons. Neuron *75*, 58–64.

Tzingounis, A.V., and Nicoll, R.A. (2008). Contribution of KCNQ2 and KCNQ3 to the medium and slow afterhyperpolarization currents. Proc. Natl. Acad. Sci. USA *105*, 19974–19979.

Wang, Z., Kai, L., Day, M., Ronesi, J., Yin, H.H., Ding, J., Tkatch, T., Lovinger, D.M., and Surmeier, D.J. (2006). Dopaminergic control of corticostriatal long-term synaptic depression in medium spiny neurons is mediated by cholinergic interneurons. Neuron *50*, 443–452.

Wilson, C.J. (2005). The mechanism of intrinsic amplification of hyperpolarizations and spontaneous bursting in striatal cholinergic interneurons. Neuron *45*, 575–585.

Wilson, C.J., and Goldberg, J.A. (2006). Origin of the slow afterhyperpolarization and slow rhythmic bursting in striatal cholinergic interneurons. J. Neurophysiol. *95*, 196–204.

Yellen, G. (2002). The voltage-gated potassium channels and their relatives. Nature *419*, 35–42.

Yue, C., and Yaari, Y. (2004). KCNQ/M channels control spike afterdepolarization and burst generation in hippocampal neurons. J. Neurosci. *24*, 4614–4624.